

From river flow to spatial flow: flow map via river extraction algorithm

Zhiwei Wei, Su Ding, Wenjia Xu, Yuanben Zhang, Yang Wang

Abstract—Flow maps are thematic maps that visualize object movements across space with a tree layout, in which the underlying tree structure is similar to a natural river system. In this paper, we present a novel and automated approach named RFDA-FM for flow maps from one origin to multiple destinations using a river extraction algorithm in digital elevation models (DEM). The RFDA-FM first models the mapping space as a flat surface by a DEM. A maze-solving algorithm (MSA) for river extraction is then adapted to calculate the flow path from one destination to the origin by constraining its searching directions, direction weights, and searching ranges according to the quality criteria of flow maps. All flow paths from the destinations to the origin are obtained iteratively based on the MSA according to their importance, which is defined by considering their length. Finally, these paths are smoothly rendered with varying widths according to their volume using Bézier curves. A comparison with existing approaches indicates that the flow maps generated by RFDA-FM can be better at keeping nodes away from edges without node overlaps and edge crosses. Two extension experiments demonstrate that RFDA-FM is applicable to heterogeneous mapping space or mapping space with obstacle areas. The parameter analysis shows that RFDA-FM can intuitively control the layouts of flow maps. Project website: <https://github.com/TrentonWei/FlowMap>

Keywords: Flow map; automatic cartography; hydrology model; maze solving algorithm; digital elevation model.

1 INTRODUCTION

Since Henry Drury Harness introduced the first flow map in 1837 [1], it has a long history of depicting migration patterns and good movements with a flow map due to its effective reduction of visual clutter and clear insight into the spatial distribution of moving phenomena [2]. Many approaches such as hierarchical clustering, edge bundling, and force-directed algorithm have been proposed [3-12]. But these works mainly focus on flow maps from multiple origins to multiple destinations. While flow maps from one origin to multiple destinations, i.e., the so-called one-to-many flow maps [2], are also widely used. Pioneers usually use an appealing tree-like layout to delineate the flow routes and volumes which is challenging to produce, thus more attention needs to be drawn to one-to-many flow map production [13].

To automate the production of a one-to-many flow map, some approaches try to generate the tree layout by bundling edges into hierarchical levels, such as the stub bundling (SB), spiral tree (ST), or force-directed (FD) approaches [2, 14-16]. But these approaches may suffer from problems of artificial feeling or low automation. The SB renders all edges as curved ones intentionally where they could be simply straight [13]. The FD requires some manual interventions, for example, the users have to manually define the force factors to obtain a satisfactory layout [15]. Though ST offers automation, it only provides a parameter “the restricting angle”

to alter the edge curvature, which is not easy to use for different user demands [13]. The other approaches generate the tree layout by simulating the motion of flows [13, 17]. For example, the river system, as natural flows across geographical regions, can also be considered a special kind of flow. Sun [13] simulates the formation of the dendritic drainage pattern of natural river systems and constructs an approximate Steiner tree to produce the one-to-many flow maps. This approach can produce a natural layout for different mapping spaces, while may generate some redundant nodes and extra operations including edge simplification and edge straightening are required. Inspired by the works of Sun [13, 17], we try to develop an approach that is automatic but intuitive for users to produce a natural one-to-many flow map by simulating the motion of flows.

River extraction is a central research task in hydrological applications, in which the digital elevation model (DEM) is usually used as a basic data model. Many approaches have been proposed in the past decades [18-31] to extract a natural river system automatically. It is intuitive to model the mapping spaces of a one-to-many flow map as DEM data, and then apply these river extraction approaches to automate its production for the following two reasons. First, since DEM is a powerful data model to represent geographic spaces [18], different mapping spaces of flow maps including the heterogeneous mapping spaces or mapping spaces with obstacle areas can be similarly represented by a DEM. Second, existing river extraction approaches such as the maze-solving algorithm (MSA) provide an intuitive way to alter the layout of a river system [25]. To this end, it would be convenient for users to alter the layout of a one-to-many flow map by applying MSA.

Motivated by the above inspirations, we propose a new, automatic approach named RDFA-FM to produce the one-

- Zhiwei Wei, Yang Wang, and Yuanben Zhang are with Aerospace Information Research Institute, Chinese Academic of Sciences and Key Laboratory of Network Information System Technology (NIST), Aerospace Information Research Institute, Chinese Academy of Sciences. E-mails: 2011301130108@whu.edu.cn, Primular@163.com, zhangyb@aircas.ac.cn.
- Su Ding is with the College of Environmental and Resource Science, Zhejiang A & F University. E-mail: suding@zafu.edu.cn.
- Wenjia Xu is with Beijing University of Posts and Telecommunications. E-mail: xuwen-jia16@mails.ucas.ac.cn.

to-many flow maps by adapting a river extraction algorithm. We model the mapping space of a flow map as a flat surface with a DEM by defining its grid type, resolution, and range based on user demands [32,33]. Then we adapt the maze-solving algorithm (MSA) to calculate the flow path from one destination to the origin, in which the searching directions, direction weights, and searching ranges of MSA are constrained according to the quality criteria of the one-to-many flow maps. Thus, the involving quality criteria or user demands can all be modeled as the properties of a DEM or the parameters of the river extraction algorithm, which enables the users to be more intuitive to produce a flow map automatically. To further improve the appearance of the flow maps, we smoothly render all flow paths using Bézier curves. Specifically, experiments using different parameter settings on three datasets with homogeneous or heterogeneous mapping spaces or mapping spaces with obstacle areas also demonstrate that the proposed approach is applicable to different mapping spaces and better at keeping nodes away from edges without node overlaps and edge crosses.

The rest of the paper is organized as follows. **Section 2** presents the approaches of the one-to-many flow maps and introduces river extraction algorithms over flat surfaces in a DEM. **Section 3** gives some definitions of the one-to-many flow maps and summarizes the quality criteria. **Section 4** illustrates the methodology of RDFA-FM. **Section 5** evaluates the RDFA-FM, and compares it with previous works. **Section 6** shows some extensions of the RDFA-FM. **Section 7** discusses the strategy effectiveness, parameter settings, and limitations of RDFA-FM. **Section 8** concludes the paper and identifies issues for future works.

2 RELATED WORKS

2.1 The one-to-many flow maps

The earliest one-to-many flow map can be traced back to Henry Drury Harness in 1837 [1]. Shortly after, Charles Joseph Minard extended this idea to depict economic topics such as the import or export of wine, cotton, and coal [34]. While these early flow maps were most drawn by hand, Tobler [35] first introduced an automatic system to produce flow maps. But straight lines were drawn from destinations to the origin with varying widths in his approach. It will result in visual clutters, which have been the main concern in later approaches.

To reduce the visual clutters, Tobler [35] introduced a filtering strategy. This strategy was also adopted by Elzen and van Wijk [36] in the interaction between flow maps. As an important strategy to reduce visual clutters in graph visualization, edge bundling is also applied for flow maps. Phan et al. [7] proposed an algorithm to bundle edges based on hierarchical clustering. But their approach may not smooth all paths and have a large total graph length. Debiasi et al. [15, 16] used the force-directed algorithm to bundle edges with node merge and node move. But it is a supervised approach and some manual interventions such as suitable force factor settings are required. Steiner tree, as a graph that connects a set of points with minimum total length by using extra points, is also widely used in flow maps [37]. Verbeek et al. [2] introduced a spiral tree by restricting the angle of a Steiner tree to produce a smooth

and crossing-free flow map. Nocaj and Ulrik [14] introduced a stub bundling strategy based on a spiral tree. But these approaches don't provide an easy-to-use way to alter the tree layout. Unlike the above approaches, Sun [13, 17] generated the flow maps by simulating the motion of flows according to the formation of the dendritic drainage pattern of natural river systems. The approach can generate a natural layout for different mapping spaces. But his approach may generate some redundant nodes and extra operations including edge simplification and edge straightening are required. Our approach is inspired by Sun [13,17] but with fewer extra operations. Compared to these edge bundling approaches, our approach may have a more natural layout and be more intuitive for users to alter the layout.

2.2 River extraction over flat surfaces in a digital elevation model

River extraction in a digital elevation model (DEM) is the key technology in hydrological applications [31]. Its process usually contains four steps: depression filling, flow direction calculation, flow accumulation, and flow track [32]. Because the elevation in a flat surface is the same, depression filling is not performed. Among the remaining three steps, flow direction calculation is the basis for the subsequent two steps. Thus, the flow directions calculation is the key process in river extraction over flat areas in DEMs, which can be categorized into two types: effectiveness first or efficiency first.

Effectiveness first algorithms aim to improve the accuracy of flow direction calculation. Due to the same elevation values within flat areas, Jensen and Domingue [18] assigned flow directions with neighborhood techniques by increasing the elevations from the outlet to the inlet. But this approach may generate parallel flows. Garbrecht and Martz [19] calculated flow directions by adding a gradient from higher to lower terrain. Because the approach of Garbrecht and Martz [19] can produce flow paths that are in line with actual situations, many approaches are then proposed to improve it [20-23]. Another basic idea for flow direction calculation is to obtain flow paths according to their importance iteratively. Tribe [24] extracted flow directions in a flat area by assuming that the main flow path was a straight line from inlet to outlet. Other flow paths were then generated iteratively by connecting them to these earlier generated flow paths. As not all paths are exactly straight lines, Zhang et al. [25] improved the approach by introducing a maze-solving algorithm (MSA) to calculate flow directions. Because we try to generate a one-to-many flow map that meets involving quality criteria as much as possible, the MSA in these effectiveness first algorithms is adopted to calculate the flow paths in our approach.

Efficiency first algorithms aim to reduce the computational cost and mainly involve strategies to reduce or speed up the calculation. For example, Zhu et al. [26] applied a neighbor-grouping scan loop strategy. While Wang and Liu

[27] presented a priority-flood algorithm that processed depressions from the edge grid cells to the interior cells. These strategies help reduce the computation complexity. Barnes et al. [28] applied different increments to flat cells in masked DEMs to avoid iterative calculation. Su et al. [29] integrated depression filling and direction assignment with a chain code matrix based on Barnes et al.'s algorithm. Their approach guides the calculation of the gradient directly from higher terrain to lower terrain instead of applying iterative searching. And a distance transform was later introduced to speed up the search process by themselves [30]. Yu et al. [31] used a "first-in, first-out" queue to process depressions and flat areas and a priority queue to process other areas which can effectively reduce the computation complexity.

3. DEFINITIONS AND QUALITY CRITERIA

3.1 Definitions

To achieve a better illustration of the proposed approach, some definitions are given. A one-to-many flow map with a tree layout connecting destinations and the origin can be represented as a graph: $G=(V, E)$, where V is the node set representing the destinations and the origin, and E is the edge set connecting two nodes in V .

Origin node. The node represents the origin, e.g., node N_1 .

Destination node. The node represents a destination, e.g., nodes N_4, N_6, N_8, N_9 , and N_{10} .

Flow-in node. The intersection node of two edges, e.g., nodes N_2, N_3, N_5 , and N_7 .

Hanging edge. The edge connects a destination node and a flow-in node, e.g., edges $N_4N_2, N_6N_5, N_8N_5, N_9N_7$, and $N_{10}N_7$.

Non-hanging edge. The edge which is not a hanging edge, e.g., N_2N_1, N_3N_2, N_5N_3 , and N_7N_3 .

Path. The route from one node to another, e.g., $N_{10}N_7N_3N_2N_1$ is a path from the destination node N_{10} to the origin node N_1 .

Volume. The amount of movement objects flowing along an edge, e.g., 100 for edge N_6N_5 and 280 for edge N_7N_3 .

Flow-in angle. The angle between an edge and its connecting non-hang edge which is with the largest volume, e.g., angle $N_1N_2N_4$.

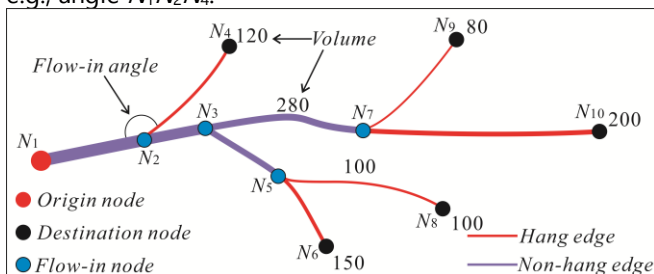


Figure 1. Definitions on the one-to-many flow maps.

3.2 Quality criteria

Design requirements of a flow map are usually

developed into quality criteria to rule its production, and different quality criteria have been developed for different purposes. For example, Debiasi et al. [15] suggested five criteria including cross-free, minimum overlaps between nodes and edges, etc. Jenny et al. [9] analyzed the design principles for flow maps with a user study and eight kinds of criteria for graph length and symmetry were proposed. Dong et al. [39] analyzed the influence of smoothness and thickness in flow maps using eye-tracking experiments. Xu et al. [40] and Holten and van Wijk [41] analyzed the balance between clarity and aesthetics by using curved edges in graph visualization. To evaluate these quality criteria, measures such as the total length of all edges, the number of edge crosses, the number of acute flow-in angles, visual smoothness index were proposed [13, 42, 43].

We summarize the quality criteria involved in the production of a one-to-many flow map as follows.

(1) Geometry

Curved edge preference (GC_1): Curved edges are preferred over straight edges in a flow map, and an edge is more likely to be rendered as a curve if possible [38, 39].

Curve difference necessity (GC_2): The users would prefer curved edges for aesthetics, but prefer straight edges for clarity in graph visualization [40]. Furthermore, the main branches of a flow map also need to be emphasized, and slightly curved edges for edges with high volume are sometimes necessary [15].

Total length minimization (GC_3): Larger total length of a flow map means a larger visual burden, and needs to be minimized [2, 13].

(2) Relation

Acute flow-in angle avoidance (RC_1): Acute flow-in angles may have negative impacts on response time, and need to be avoided [44, 45].

Edge cross avoidance (RC_2): Edge crosses may lead to confusion, and need to be avoided [2, 13, 15].

Overlap avoidance between nodes and edges (RC_3): Overlaps between destination nodes and edges may lead to visual clutters, and need to be avoided [2, 13, 15].

Cross avoidance between edges and important map objects (RC_4): Some map objects may be important and the edges need to avoid these important map objects to aid recognizability [2, 13].

Suitable distance between nodes and edges (RC_5): The destination nodes should be far away enough from the edges for clarity [13].

(3) Distribution

Tree layout (DC_1): The destination nodes should be grouped into hierarchical levels and represented as a tree layout, where the origin is the root node and the destinations are leaf nodes; and edge widths of the flow map are then drawn atop thick ones to the thin ones according to the hierarchy [2, 13, 15].

On the one hand, the quality criteria summarized above may conflict with or enhance one another. For example, though curved edges are preferred (GC_1), straight lines or slightly curved lines for edges with high volume are also necessary (GC_2); and keeping a suitable distance between nodes and edges (RC_5) will also avoid the overlaps between nodes and edges (RC_3). On the other hand, the quality

criteria may have different priorities. For example, overlap or cross avoidance (RC_2 , RC_3 , and RC_4) may have higher priorities than the total length minimization (GC_3). Because the overlaps or crosses must be avoided, while the total length minimization only needs to be satisfied as much as possible. Thus, the quality criteria in a one-to-many flow map are not like those in the database domain which should be satisfied completely, they only need to be optimized or fulfilled as much as possible [46].

4 METHODOLOGY

4.1 Framework

The proposed approach (RFDA-FM) tries to adapt a river extraction algorithm over flat surfaces in a digital elevation model (DEM) to produce the one-to-many flow maps by considering their quality criteria, and RFDA-FM consists of three steps.

Step 1. Modeling the mapping space as DEM data: The mapping space is modeled as DEM data over a flat surface by defining its grid type, resolution, and range based on user demands. The destination nodes and the origin node are represented by their corresponding grids, and the destination grids have an outflow that eventually gathers in the origin grid.

Step 2. Flow path calculation: The maze-solving algorithm (MSA) is applied to calculate the flow path from one destination grid to the origin grid by constraining its searching directions, direction weights, and searching ranges according to the quality criteria of flow maps. All flow paths from the destination grids to the origin grid are obtained iteratively according to their importance, which is defined by their length.

Step 3. Flow render: The edges are rendered smoothly with varying widths according to their flow volumes by using Bézier curves for aesthetic purposes.

4.2 Step 1. Modeling the mapping space as DEM data

The digital elevation model (DEM) is a representation of the elevation in a continuous terrain surface via irregular or regular grids with a certain resolution, in which the grid type, resolution, and range need to be defined [42]. Thus, we model the mapping space of a flow map as DEM data by defining its grid type, resolution, and range. Because the mapping space of a flow map is usually considered uniform, the mapping space is modeled as a flat surface, which means the grids are all with the same elevation values.

Suppose the origin node O and destination nodes N_n are represented as $NS = \{O, N_1, \dots, N_n, \dots\}$, where N_n has a property f_n which represents the flow volume from N_n to O . The regions as a base map are $RegS = \{R_1, R_2, \dots, R_m, \dots\}$, where R_m is a region. The grid type, resolution, and range of the DEM are defined as follows (Figure 2).

(1) **Grids.** Regular grid (square) is adopted by considering its lower computational cost and common uses (Figure 2) [42].

(2) **Resolution.** The resolution needs to make sure that the two closest nodes in the node set (NS) do not fall into the same grid. But a higher resolution means a higher computational cost [42]. According to the detailed analysis of

resolution setting in spatial applications by Hengl [47], the resolution (R_s) of the DEM is defined by considering the shortest distance between nodes in NS as Equation (1).

$$R_s = \frac{AveMinD_{(5\%)}}{4} \quad (1)$$

Where $AveMinD_{(5\%)}$ is the average distance between the first 5% of the closest node pairs in NS .

(3) **Range.** The range of the DEM data can be set according to the envelope of the node set (NS) or the regions as a base map ($RegS$), e.g., the range is defined as the envelope of $RegS$ in Figure 2. When the range is defined according to the envelope of NS , the range needs to extend a half grid out to prevent nodes in NS from locating on the boundary of the defined range. The two definitions are both available and up to users in practice.

(4) **Modeling the obstacle areas or important objects:** The flow paths sometimes need to avoid obstacle areas or important objects [2,13]. For example, areas with bad weather may need to be avoided while mapping good movements. Thus, grids within these areas need to be deleted from the existing range, e.g., the grids colored red in Figure 2. Based on a similar idea, point, linear, or planar obstacle areas or important objects can all be represented by deleting corresponding grids in our approach (Figure 2). Then cross avoidance between edges and important map objects (RC_4) can be satisfied.

(5) **Modeling the heterogeneous mapping space.** Area differences may sometimes be considered by users. For example, bypassing land areas may have a higher travel cost than sea areas while mapping good movements [2, 13]. Two strategies are available and up to users in practice: 1) Different areas are represented as grids with different types; 2) Different areas are represented as grids with different resolutions [31]. As shown in Figure 2, the areas within the regions as a base map ($RegS$) are assigned as Type 2 grids, while the other areas are assigned as Type 1 grids. By defining different types of grids, the areas within $RegS$ or not are distinguished.

With the above definitions, the mapping space is then modeled as DEM data over a flat surface. Each node in the node set (NS) can be represented by its corresponding grid as $GS = \{OG, G_1, \dots, G_n, \dots\}$. Where OG is the grid representing the origin node, and G_n is the grid representing the destination node N_n .

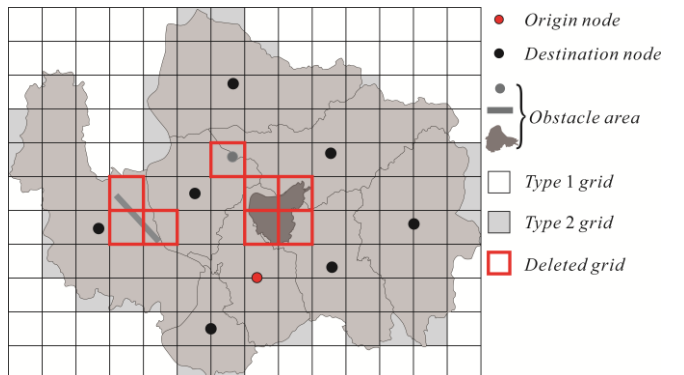


Figure 2. Modeling the mapping space of a flow map as DEM data over a flat surface.

4.3 Step 2. Flow path calculation

According to the illustrations in **Section 2.2**, the river extraction calculation in hydrological applications is usually implemented by generating the river paths iteratively according to their importance, in which a less important river path is generated by connecting it to an earlier generated river path. A potential river path from a destination to the origin is defined as a path with the shortest length and is obtained with a maze-solving algorithm (MSA) [24]. Thus, three keys are involved: (1) The path length definition, (2) the MSA, and (3) the path importance definition.

The quality criteria of the one-to-many flow maps need to be optimized or fulfilled as much as possible, as analyzed in **Section 3.2**. Thus, the iterative process for river path calculation is acceptable for flow path calculation in a one-to-many flow map to achieve local optimization. (1) The path length definition, (2) the MSA, and (3) the path importance definition are adapted to calculate the flow paths of a one-to-many flow map by considering its quality criteria as following sections.

4.3.1 Path length definition

The length of a path from a destination grid to the origin grid can be computed according to its flowing through grids. Thus, the length between two neighborhood grids is defined first. The length of a path is then defined by considering the quality criteria of the one-to-many flow maps.

4.3.1.1 Length definition between two neighborhood grids

The grids may have different types if the mapping space is heterogeneous, and can be assigned different weights (as defined in **Section 4.2**). The length (NL) between two neighborhood grids (G_m and G_n) is defined as Equation (2), as shown in Figure 3.

$$NL = \begin{cases} 0.5R_s \times \delta_m + 0.5R_s \times \delta_n & (\text{Orthogonal neighbors}) \\ \sqrt{2} \times (0.5R_s \times \delta_m + 0.5R_s \times \delta_n) & (\text{Diagonal neighbors}) \end{cases} \quad (2)$$

Where R_s is the resolution of the DEM data (defined in **Section 4.2**), δ_m and δ_n are the weights of G_m and G_n and can be set by users. If the mapping space is considered homogeneous, grids are all the same type and $\delta_m = \delta_n = 1$.

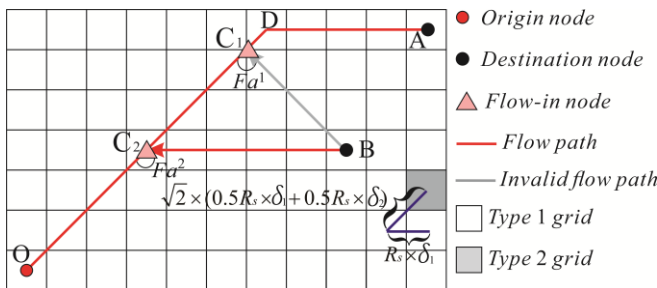


Figure 3. Path length definition. If only the total length minimization requirement (GC_3) is considered, the path BC_1O is preferred over BC_2O because C_1O and C_2O are not newly generated sub-paths, and the newly generated sub-path BC_1 is shorter than BC_2 . If the acute flow-in angle avoidance (RC_1) is also considered, the path BC_2O is preferred over BC_1O because the length of the path BC_1O is penalized for its acute flow-in angle.

4.3.1.2 Path length definition and refinement

The paths from the destination grids to the origin grid

are generated iteratively in our approach. Suppose the earlier generated paths are $FpS = \{Fp_1, Fp_2, \dots, Fp_n, \dots\}$, Fp_n is an earlier generated path from a destination grid (G_n) to the origin grid (OG). For a newly given destination grid (G_i), a potential path (Fp_i) from G_i may flow in any grid of $Fp_n \in FpS$ to OG . Because the valid flow path from G_i to OG is defined as a path with the shortest length in hydrological applications [24]. Thus, when we try to obtain the valid path from G_i to OG , we need to find all the shortest paths ($CacheFpS$) from G_i that flow in each grid of $Fp_n \in FpS$ with the maze-solving algorithm (MSA) first. And the valid path from G_i to OG should be the shortest one in $CacheFpS_i$. Thus, if Fp_i violates a quality criterion in **Section 3.2**, it will have a larger length and be less likely to be the valid path from G_i to OG and vice versa. Two quality criteria, total length minimization (GC_3) and acute flow-in angle avoidance (RC_1), are considered here for path length definition.

(1) Path length definition by considering the total length minimization (GC_3)

For a potential path (Fp_i) from a destination grid (G_i) to the origin grid (OG), Fp_i can be divided into two parts: $sub-Fp^1_i$ and $sub-Fp^2_i$, where $sub-Fp^2_i$ is a sub-path of $Fp_n \in FpS$ and is not newly generated, and $sub-Fp^1_i$ is newly generated. Then a shorter $sub-Fp^1_i$ will help minimize the total length (GC_3). For example, the two paths (BC_1O and BC_2O) in Figure 3 that separately flow in an earlier generated path (ADO) at grid C_1 and C_2 can both be a path from the destination grid B to the origin grid O. Because C_1O and C_2O are both parts of an earlier generated path (ADO), but the sub-path BC_1 of BC_1O is shorter than the sub-path BC_2 of BC_2O . If the total length minimization requirement (GC_3) is considered, BC_1O is more likely to be the valid path from destination grid B to origin grid O due to a smaller total length. This means that the length of $sub-Fp^1_i$ should be more important than the length of $sub-Fp^2_i$ in the path length definition if GC_3 is considered. Then the length (PL) for Fp_i is defined as Equation (3).

$$PL_i = subPL^1_i + subPL^2_i \times \omega \quad (3)$$

Where $subPL^1_i$ and $subPL^2_i$ are the lengths of $sub-Fp^1_i$ and $sub-Fp^2_i$, ω is a weight and $\omega \leq 1$, it means $subPL^1_i$ is more important than $subPL^2_i$.

(2) Path length refinement by considering the acute flow-in angle avoidance (RC_1)

The acute flow-in angle avoidance (RC_1) rules that acute flow-in angles (Fa , defined in **Section 3.1**) need to be avoided. Whether a Fa is an acute one is defined by setting a threshold (T_a): If $Fa \leq T_a$, then Fa is an acute one. If a potential path (Fp_i) from a destination grid (G_i) to the origin grid (OG) flows in an earlier generated path with an acute flow-in angle, a penalty strategy is applied to refine its length. Thus, Fp_i is less likely to be the shortest (or valid) one from G_i to OG . The path length refinement is defined as Equation (4).

$$PL_i = PL_i + PL_{pen} \quad (4)$$

Where PL_i is the length of Fp_i , PL_{pen} is a large constant and set as $PL_{pen} = 20R_s$ in this approach. For example, the two paths BC_1O and BC_2O in Figure 3 can be both a path from the destination grid B to the origin grid O. But the path BC_1O flows in an earlier generated flow path (ADO) at grid C_1 with an acute flow-in angle (Fa^1). Then the path length

of BC_1O is penalized by Equation (4), and BC_2O is finally obtained as the shortest path from destination grid B to origin grid O because its flow-in angle ($F\alpha^2$) at grid C_2 is not an acute one.

4.3.2 The maze-solving algorithm

Maze solving is a classical problem in graph theory and data structure fields. As it aims to find the shortest path between the entrance to the outlet in a given labyrinth, which has been applied to generate river paths in digital elevation model (DEM) data successfully [25]. The flat surface is considered as a labyrinth without inside walls, the destination grid is considered an entrance, and the origin grid is considered an outlet. Three definitions are required in a maze-solving algorithm (MSA): (1) searching directions, (2) direction weights, and (3) searching ranges [48]. Searching directions determine the potential directions to be searched. Direction weights determine which direction is first to be searched. Searching ranges determine where can be searched. They are defined by considering the quality criteria in Section 3.2.

4.3.2.1 Searching direction definition

Searching directions determine the potential directions to be searched. As a grid in DEM, its outflow direction to its neighborhood grids can be 8 directions (8D), denoted as $8D = \{0, 1, 2, 3, 4, 5, 6, 7\}$ [49]. However, it is time-consuming if all directions are explored each time and it might be more suitable to only search in the directions towards the target grid. As shown in Figure 4, the searching directions might be $\{0, 1, 2\}$ while searching from grid A to grid N, and $\{2, 3, 4\}$ while searching from grid B to grid N.

Given a start grid as G_i , the target grid that G_i searches towards is G_j , and the angle between the line G_iG_j which connects G_i and G_j and the horizontal direction is $Angle_{ij}$. The searching directions ($sDir_{ij}$) from G_i to G_j are defined as Equation (5).

$$sDir_{ij} = \{x | x = y \bmod 8, y \in \{z-1, z, z+1\}, z = \lfloor Angle_{ij} / 45 \rfloor\} \quad (5)$$

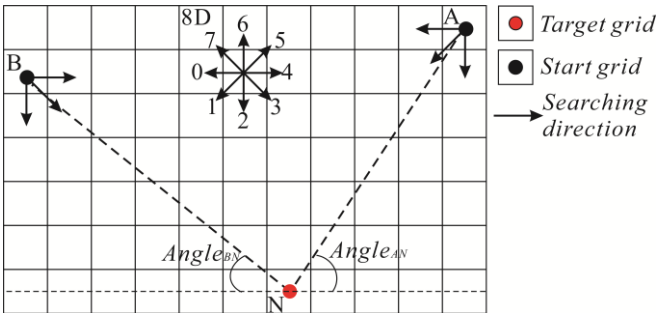


Figure 4. Searching direction definition. It only searches in the directions from the start grid toward the target grid to improve efficiency.

4.3.2.2 Direction weight definition

Direction weights determine which direction is first to be searched. Direction weights in digital elevation models (DEM) are usually assigned as the downward slope angle of neighborhood grids, which are defined according to the distance and elevation value difference between two neighborhood grids [19]. As the mapping space is modeled as a flat surface in this approach, and grids are all with the same elevation values. Then the elevation value difference

between the two neighborhood grids is 0. To overcome this problem, the idea according to river system extraction in DEM data that the grid with higher flow accumulation is more likely to be mainstream is adopted. This idea can also help generate a more suitable tree layout (DC_1) and minimize the total length (GC_3) [25].

The grid with higher flow accumulation is more likely to be mainstream, which means the direction toward a grid that has a larger potential flow accumulation is prior to be explored. The potential flow accumulation (Pf_i) of a grid (G_i) can be calculated by the total volume of the grids in its k -order surrounding and is defined as Equation (6) [25].

$$Pf_i = \sum_{\substack{x \leq m+k, y \leq n+k \\ x = m-k, y = n-k}} f_{xy} \quad (6)$$

Where G_i is a grid in row m and column n in the DEM data, f_{xy} is the volume of the grid in row x and column y . Given two neighborhood grids as G_i and G_j , the direction weight (DW_{ij}) for the direction from G_i to G_j is defined as Equation (7) [19, 25]

$$DW_{ij} = \begin{cases} (Pf_i - Pf_j + Tf) / NL_{ij} & (Pf_i - Pf_j > 0) \\ Tf / NL_{ij} & (Pf_i - Pf_j \leq 0) \end{cases} \quad (7)$$

Where Pf_i and Pf_j are the potential flow accumulation of G_i and G_j , Tf is a constant, and $Tf \in R^+$ in case $Pf_i - Pf_j \leq 0$, NL_{ij} is the length between G_i and G_j (defined as Equation (2)).

As shown in Figure 5, the two paths (AEDO and ACFO) may both be as a path from destination grid A to the origin grid O if the potential flow accumulation (P_f) of each grid is not considered. But the path ACDO is finally obtained as a path from destination grid A to the origin grid O by considering the P_f of each grid. Though ACDO is of the same length as AEDO and ACFO, it is clear in Figure 5 that more destination grids are more likely to connect ACDO with shorter paths than to connect AEDO and ACFO. Thus, the direction weight definition with Equation (7) will help generate a more suitable tree layout (DC_1) and minimize the total length (GC_3).

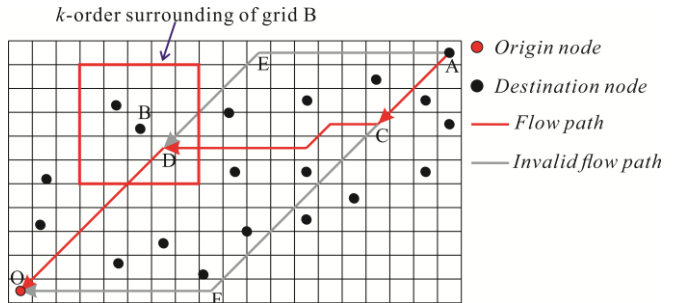


Figure 5. Direction weight definition. The searching direction toward a grid that has a larger potential flow accumulation is prior to be explored.

4.3.2.3 Searching range definition

The maze-solving algorithm (MSA) is performed with defined directions and direction weights in a searching range to obtain the shortest path between two grids. If certain grids are excluded from the searching range, then the path obtained between two grids by MSA will never flow through the certain grids, namely, no overlaps or crosses will be made on these grids. As shown in Figure 6, if we exclude grid B in the searching range while we try to obtain a path from the destination grid A to the origin grid O with

the MSA, then all the potential paths from the destination grid A to the origin grid O will never overlap grid B.

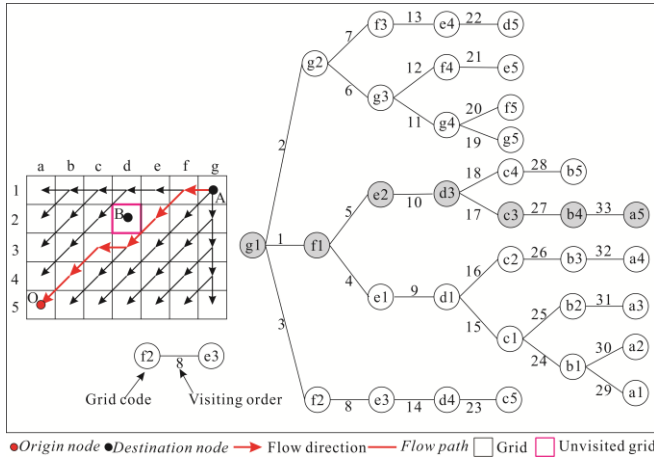


Figure 6. An example of the shortest path calculation with the maze-solving algorithm (MAS) in a defined searching range. Grid B is excluded from the searching range, and all the potential paths from grid A to grid O will never cross or overlap grid B.

The quality criteria in **Section 3.2** rule that overlaps between nodes and edges should be avoided (RC_3) and suitable distance between nodes and edges should be maintained (RC_5). As the example shown in Figure 6, if we exclude the grids representing target nodes in the searching range, the obtained paths with the maze-solving algorithm (MSA) will never overlap the target nodes. Because the paths may be rendered with varying widths and suitable distances also need to be maintained between nodes and edges. We can exclude the t -order surrounding of specific grids from the searching range to satisfy RC_3 and RC_5 , where two situations need to be specifically considered.

(1) Special consideration for $t=1$

The destination nodes may not be exactly in the center of their representing grids, e.g., the destination node in grid B in Figure 7(a). Because the destination node in grid B locates near the boundary of its representing grid, the distance between the obtained path ACO and the node in grid B may be small though the path does not overlap grid B with $t=1$. To maintain suitable distances between nodes and edges with $t=1$, we define 1-order surrounding (1- SG) for a grid (G_i) representing a node (N) as Equation (8).

$$1-SG_i = \{G_{xy} | m-1 \leq x \leq m+1, n-1 \leq y \leq n+1, HDis(G_{xy}, N_i) < 0.5R_s, VDis(G_{xy}, N_i) < 0.5R_s\} \quad (8)$$

Where G_i is a grid in row m and column n in the digital elevation model (DEM) data, G_{xy} is a grid in row x and column y , R_s is the resolution of the DEM data (defined as equation (1)). $HDis(G_{xy}, N_i)$ and $VDis(G_{xy}, N_i)$ are the minimum distances between grid G_{xy} and node N_i in horizontal and vertical directions. The defined 1-order surrounding for grid B is shown in Figure 7(a).

(2) Special consideration for particularly close destination nodes

If the destination nodes are close enough, then a given destination grid (G_i) may be in the t -order surrounding of another grid. Then G_i will be excluded from the searching range according to our definition, and no available paths

can be obtained from G_i to the origin grid (OG). Thus, smaller t is adaptively set for these grids in our approach to avoid G_i being excluded from the searching range. As shown in Figure 7(b), grid A is in a 2-order surrounding of grid B. If we set $t=2$ while we try to obtain a path from grid A to the grid O with the maze-solving algorithm (MAS), grid A will be excluded from the searching range and no available paths can be obtained from grid A to grid O. Thus, $t=1$ is adaptively set for grid B on this occasion.

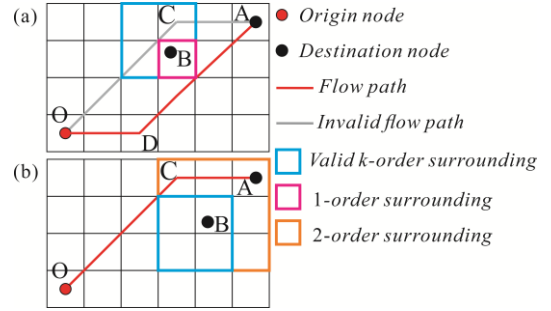


Figure 7. Special considerations for searching range definition. (a) Special consideration for $t=1$: the grids colored cyan are the defined 1-order surrounding of grid B; (b) Special consideration for close destination nodes: t is adaptively set from $t=2$ to $t=1$ for grid B because grid A is in 2-order surrounding of grid B.

4.3.3 Path importance

River importance is usually determined by its length and flow volume [25]. As ruled by the total length minimization (GC_3), the path length may be the first to be considered. Thus, the importance (FP_{im}) of a flow path (Fp_i) is defined by considering its length in our approach. Because the paths are generated iteratively in this approach, supposed the earlier generated flow paths are $FpS = \{Fp_1, Fp_2, \dots, Fp_n, \dots\}$, Fp_n is a path from a destination grid (G_n) to the origin grid (OG). For a newly generated path (Fp) from a destination grid (G_i) to OG , Fp_i can be classified into two types by considering whether its sub-path is part of $Fp_n \in FpS$, as follows.

Type I flow path: if no sub-path of Fp_i is a part of $Fp_n \in FpS$, then Fp_i is a type I path.

Type II flow path: If there exists a sub-path of Fp_i is a part of $Fp_n \in FpS$, then Fp_i is a type II path.

If Fp_i is a type I path, it means that Fp_i from the destination grid straightly connects to the origin grid. Then Fp_i is more likely to be another mainstream according to the river system extraction process in hydrological applications [25]. Thus, the type I path is considered more important than a type II path, and the path importance (FP_{im}) of Fp_i is defined as Equation (8).

$$FP_{im} = \begin{cases} PL_i + PL_{lim} & \text{(Type I Path)} \\ PL_i & \text{(Type II Path)} \end{cases} \quad (8)$$

Where PL_i is the length of Fp_i and PL_{lim} is a large constant to make sure that a type I path is more important than a type II path, and $PL_{lim} = 10000R_s$ in this approach.

4.3.4 Iterative process for flow path calculation

Given the origin grid (OG) and destination grids (G_n) as $GS = \{G_1, \dots, G_n, \dots\}$ in modeling DEM data according to **Section 4.2**, the flow paths from all destination grids to the origin grid are generated iteratively as **Algorithm 1**.

Because the flow path from a destination grid to the origin grid is defined as a path with the shortest length, and the path with the largest importance is selected iteratively. Thus, the iterative process can naturally avoid edge crosses (RC_2) according to the river extraction process [18, 19].

Algorithm 1: Flow path calculation

Input: The origin grid is OG , destination grids are $GS = \{G_1, \dots, G_n, \dots\}$, and the DEM data represents the mapping space.

Output: Flow paths from $G_n \in GS$ to OG as $FpS = \{Fp_1, Fp_2, \dots, Fp_n, \dots\}$

Initialization: The output flow paths as $FpS = Null$, the grids representing the paths in FpS as $FGS = Null$, and the two cache flow paths as $CacheFpS_1 = Null$ and $CacheFpS_2 = Null$, $CacheFpS_1$ records the all shortest paths from each destination grid to OG , $CacheFpS_2$ records the all potential path from a given destination grid to OG .

While GS **Not** $Null$ **Do:**

Set $CacheFpS_1 = Null$;

Foreach $G_n \in GS$ **Do:**

Set $CacheFpS_2 = Null$;

Foreach $G_m \in FGS$ **Do:**

Get flow path (Fp) with the shortest 'path length' from G_n to OG which flows in a path in FpS at grid G_m with 'the maze solving algorithm'; add Fp_i to $CacheFpS_2$;

Get the path (Fp) with the shortest 'path length' in $CacheFpS_2$ and add it to $CacheFpS_1$;

Get the path (Fp_l) with the largest 'path importance' in $CacheFpS_1$ and add it to FpS ; Update the grids in FGS ; Remove the corresponding destination grid of Fp_l from GS

Return FpS

4.4 Step 3. Flow render

After all flow paths are obtained, we render the flow paths with varying widths according to their volumes. To further improve their appearance, a smooth process is implemented to render these flow paths as curves.

4.4.1 The edge widths

The width of an edge is set as the common practice in other works [2, 13-17], being proportional to its volume which can be obtained based on the flow accumulation of its flowing through grids. As shown in Figure 8(a), the flow accumulation of a certain grid is the total amount of the flow volume which gathers at the grid and can be obtained based on the calculated flow paths. The result to render the flow paths with varying widths is shown in Figure 8(b).

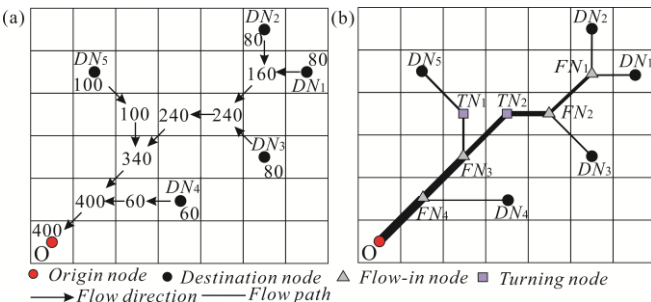


Figure 8. The edge widths. (a) Flow accumulation of each grid; (b) The edges are rendered with their widths being proportional to their flow volume.

4.4.2 Smooth process

We use the Bézier curve to smooth the edges according to Sun [13] by considering the curved edge preference (GC_1) and curve difference necessity (GC_2). Because the edges are rendered with varying widths, the flow-in locations may become not smooth, e.g., the locations at flow-in nodes FN_1 , FN_2 , FN_3 , and FN_4 in Figure 8(b). Thus, the nodes at these flow-in locations are shifted first and smooth operations are then implemented.

(1) Node shifts at the flow-in locations

To enable smoothness at the flow-in locations, the nodes of a branch edge connecting its main branch are shifted with a distance in a direction that is perpendicular to the vector of its connecting main branch [15, 16]. The shifted distance (Sd) is decided by all edges involving the flow-in locations. Given a flow-in node as N_n , the edges which flow in N_n are arranged in a clockwise order as $ES = \{E_1, E_2, \dots, E_i, \dots\}$, the width of E_i is W_i and the width of the main branch is W_{main} . The shifted distance (Sd) of the flow-in node for a given edge (E) is defined as Equation (9) (Figure 9).

$$Sd = \sum_{j=0}^{i-1} W_j + 0.5 * W_i - 0.5 * W_{main} \quad (9)$$

Here the shifted distance (Sd) is graphic and is computed based on the widths of the edges. Because flow maps are mainly applied to visualize object movements across geographic spaces. If scale or projection is considered in a flow map, Sd needs to be converted into geographic distance. We have offered a tool to convert graphic distance to geographic distance in our uploaded code.

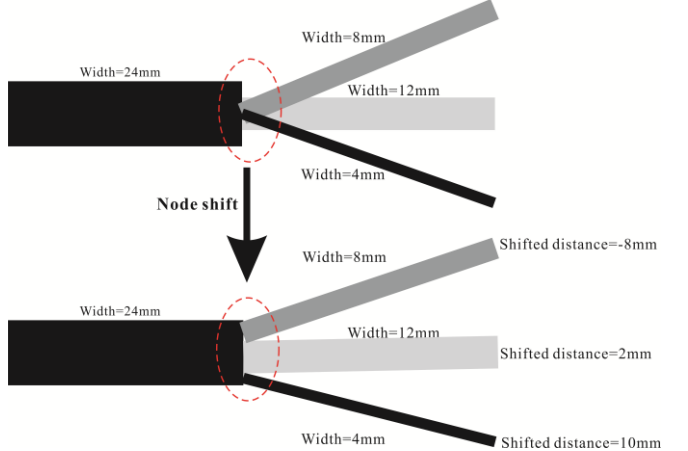


Figure 9. Node shifts at the flow-in locations.

(2) Smooth the edges with Bézier curves

We smooth the edges with Bézier curves by mainly considering the curved edge preference (GC_1) and curve difference necessity (GC_2). GC_1 rules that an edge is more likely to be rendered as a curve if possible. While GC_2 rules that the main branches of the flow map need to be emphasized, slightly curved lines for edges with high volume are also necessary. Here the non-hanging edges can all be considered as the main branches. Thus, the hanging edges are smoothed as regularly curved lines, and the non-hanging edges are smoothed as slightly curved lines. Furthermore,

because the edges are rendered with varying widths, the smooth process also needs to enable smoothness at the flow-in locations.

A Bézier curve is drawn by defining its controlling nodes [13]. The start node, turning nodes and end node of a given edge (E_i) can be considered as the initial controlling nodes of the Bézier curve, and two new controlling nodes need to be inserted for E_i to create curved lines. Suppose the controlling nodes of E_i are $CNS = \{N_1, N_2, \dots, N_n, \dots, N_e\}$, where N_1 is the start node of E_i , N_n is a turning node of E_i , N_e is the end node of E_i , and the vector of E_i 's connecting main branch is \overline{vec}_i . Two new controlling nodes are inserted as follows.

The first inserted controlling node (N_p): N_p is inserted for E_i to enable smoothness at the flow-in locations. N_p is inserted by making the distance of $N_1 N_p$ (Dis_{1p}) as $Dis_{1p} = setDis$, $N_1 N_p$ is in direction of \overline{vec}_i , as shown in Figure 10(b). $setDis$ is a small constant and is set as $setDis=0.2R_s$ in our approach (R_s is the resolution of the DEM data).

The second inserted controlling node (N_q): N_q is inserted to control the curvature level of the curve by considering whether the given edge (E) is a hanging edge or not: If E_i is a hanging edge, N_q is added by making the distance of $N_1 N_q$ (Dis_{1q}) as $Dis_{1q} = \alpha * Dis_{12}$, $N_1 N_q$ is in direction of \overline{vec}_i ; If E_i is a non-hanging edge, N_q is added by making the distance of $n_1 n_q$ (Dis_{1q}) as $Dis_{1q} = \beta * Dis_{12}$, $n_1 n_q$ is in direction of \overline{vec}_i , as shown in Figure 10(b). Where α and β are constants, Dis_{12} is the length of $N_1 N_2$, $\alpha=0.5$ to make sure the rendered line is a regular curved one, and $\beta=0.1$ to make sure the rendered line is a slightly curved one, α and β can also be set by users to control the edge curvature. Because the given edge (E_i) may have turning nodes, and three nodes are enough to draw a Bézier curve. If the number of the initial controlling nodes of E_i is not less than 3, we won't insert a second controlling node for E_i e.g., the second controlling nodes are not inserted for edges $FN_3 TN_2 FN_2$ and $FN_3 TN_1 DN_5$ in Figure 10 (b).

5 EXPERIMENTS

5.1 Experimental settings

(1) Datasets

In this paper, we take the population migrations from Texas to other states in the 2000 US Census as experiment data, which has been a widely used benchmark dataset for flow map production [2, 13-17], and comparisons are then made. Data source as: <https://www.ipums.org/>.

Two other datasets are also taken as experimental data in extensions of our approach, in which mapping spaces with obstacle areas and heterogeneous mapping spaces are considered. They will be illustrated in Section 6.

(2) Parameter settings

Three parameters need to be set in our approach.

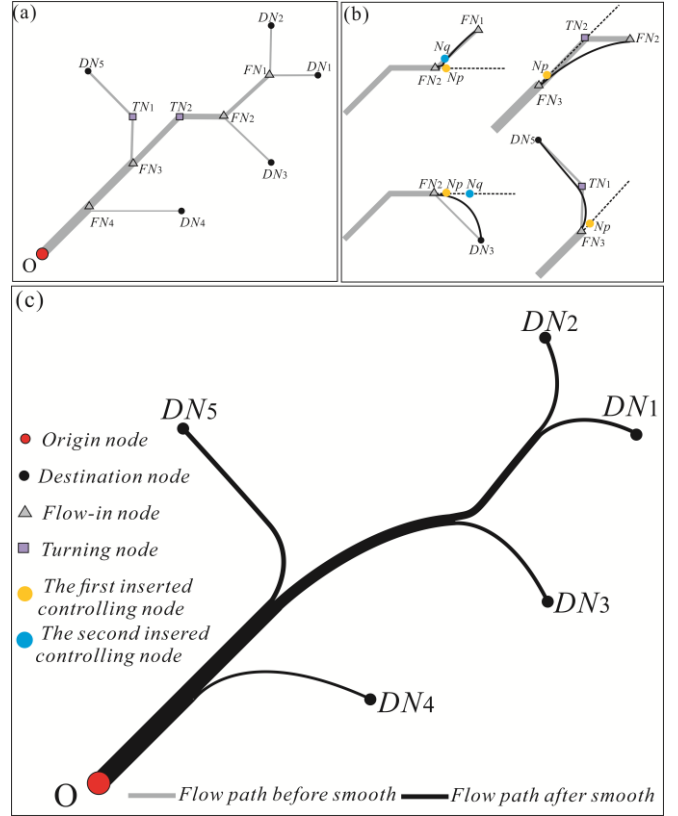


Figure 10. Flow smooth. (a) The flow paths before smooth; (b) Inserted controlling nodes; (d) The flow paths after smooth.

The parameters to generate the flow map for evaluations are set according to experiments as follows: $\omega=0.65$ in Equation (3), $k=4$ in Equation (6), and $t=1$ in searching range definition by considering overlap avoidance and suitable distance maintenance between nodes and edges (RC_3 and RC_5).

The influence of the parameter settings on flow map layouts will be discussed in detail in Section 7.2. Two other layouts with different parameter settings will be displayed in comparison with other approaches, and more layouts with different parameter settings will be displayed in Sections 7.1 and 7.2.

(3) Evaluation metrics

The resulting quality is evaluated according to the quality criteria in Section 3.2. The metrics are adopted as follows [13, 42, 43].

The mean value of visual smoothness index (MSI): Visual smoothness index (S) is a metric which is proposed by Sun [13]. S gives high values to the smooth edges with small splitting angles and punishes unnecessary bends and large curvature. Therefore, visually smooth and natural edges will have high values. The mean value of S (MSI) for all edges is adopted to evaluate the curved edge preference (GC_1) and curve difference necessity (GC_2).

The total length of the flow map (TL): TL is used to evaluate the total length minimization (GC_3).

The number of acute flow-in angles (FaN): FaN is used to evaluate the acute flow-in angle avoidance (RC_1). Acute flow-in angle (Fa) is defined by setting a threshold (T_a) for Fa . If $Fa \leq T_a$, then Fa is an acute one, and $T_a=120$ in our approach.

The number of edge crosses (ECM), the number of overlaps between nodes and edges (EON), and the number of crosses between edges and important objects (EIN): ECN , EON , and EIN are used to evaluate the overlap or cross avoidance (RC_2 , RC_3 , and RC_4).

The minimum distance between nodes and their nearby edges ($MDis$): $MDis$ is used to evaluate the suitable distance maintenance between nodes and edges (RC_5) according to Sun[13].

The mean value of user preference index ($MUPI$): user preference index (UPI) is a preference value rated by users for a flow map layout. The mean value of UPI is used to evaluate whether a flow map layout is preferred by users (DC_1). UPI is obtained by asking 23 participants to rate how much they liked the layout with a 5-point scale. 1 means "very dislike", 2 means "dislike", 3 means "Neither dislike nor like", 4 means "like", and 5 means "very like". The participants are postgraduate or undergraduate students from Wuhan University, and they all major in cartography or geographic information system.

5.2 Results and evaluations

The generated flow maps (RFDA-FM₁) for population migration from Texas to other states in the 2000 US Census with given parameter settings are shown in Figure 11. The statistical results are shown in Table 1. From Figure 11 and Table 1, we have the following observations: (1) All edges are rendered with varying widths according to their volumes, and they are smoothed by using Bézier curves and MSI is 0.751 (GC_1 and GC_2 are satisfied). (2) No acute flow-in angles are made (RC_1 is satisfied); (3) No edge crosses are made (RC_2 is satisfied); (4) No overlaps between nodes and edges are made (RC_3 is satisfied); (5) The minimum value of $MDis$ is $47.6 \times 10^3 m$ and 14 nodes are with their $MDis$ less than $100 \times 10^3 m$, these mean that suitable distances can also be maintained between nodes and edges (RC_5 is satisfied); (6) $MUPI$ is 3.30 out of 5 (5 being the optimal value), which mean that most of the users moderately prefer the generated flow map (DC_1 is satisfied). With the above observations, we can conclude that the flow map generated with our approach can well meet all the quality criteria in Section 3.2.

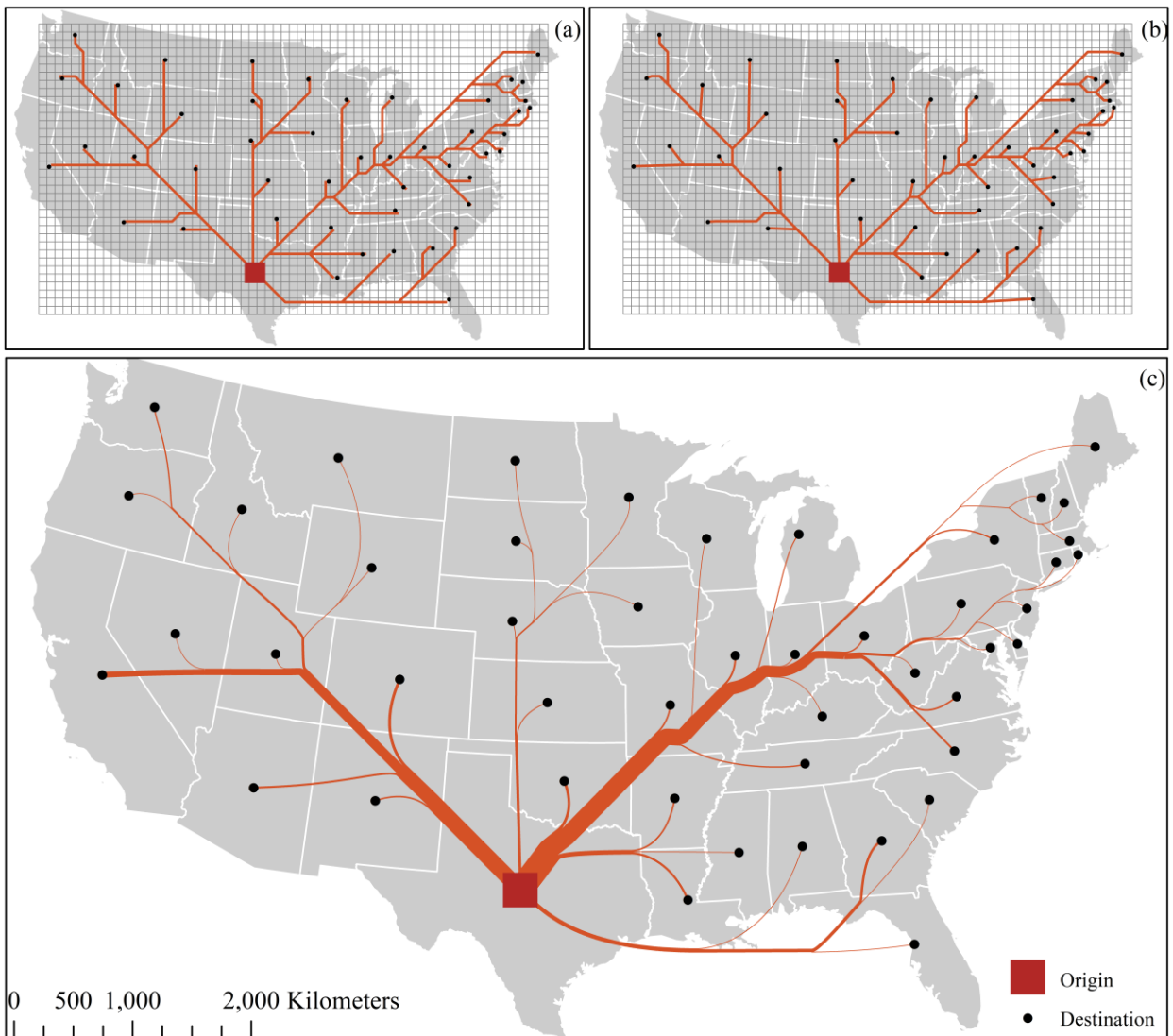


Figure 11. Flow map for population migration from Texas to other states in 2000 US Census. (a) Flow directions in the digital elevation model (DEM); (b) Flow paths in which the nodes are connected based on the calculated flow directions; (c) Flow map in which the flow paths are smoothed and rendered with varying widths (RFDA-FM₁).

Table 1. Quantitative assessment on layout quality.

<i>Measures</i>	<i>RFDA-FM₁</i>	<i>RFDA-FM₂</i>	<i>RFDA-FM₃</i>	<i>FD</i>	<i>ST</i>	<i>SB</i>	<i>TNSS</i>
<i>TL</i> (10 ⁶ m) ↓	24.63	22.58	25.03	23.61	22.01	24.46	25.59
<i>MSI</i> ↑	0.751	0.758	0.769	0.625	0.621	0.698	0.726
<i>MDis</i> (10 ³ m)							
<i>MDis_{min}</i> ↑	47.6	52.5	38.9	7.8	49.7	13.0	37.7
<i>n</i> (<i>MDis</i> <100) ↓	15	17	6	29	27	28	15
<i>n</i> (<i>MDis</i> <70) ↓	8	8	4	27	14	17	2
<i>n</i> (<i>MDis</i> <40) ↓	0	0	1	5	0	10	0
<i>n</i> (<i>MDis</i> <20) ↓	0	0	0	1	0	1	0
<i>FaN</i> (<120°) ↓	0	0	0	1	0	0	4
<i>ECN</i> ↓	0	0	0	0	0	0	0
<i>EON</i> ↓	0	0	0	1	0	0	0
<i>MUPI</i> ↑	3.30	3.04	3.43	3.13	3.26	3.52	3.39

Note: RFDA-FM is the new approach proposed in this article, where RFDA-FM₁ is Figure 11(c), RFDA-FM₂ is Figure 12(e), and RFDA-FM₃ is Figure 12(f); FD is the force-directed approach [15], Figure 12(a); SB is the stub bundling approach [14], Figure 12(b); ST is the spiral tree approach [2], Figure 12(c); TNSS is the flow motion simulation approach [13], Figure 12(d). Some statistics in Table 1 for TNSS, ST, SB, and FD are from Sun [13].

5.3 Comparisons

To validate the feasibility and generalization ability of the proposed approach (RFDA-FM), we compared the obtained flow maps with the proposed approach to existing approaches, including the force-directed approach (FD) [15], the spiral tree approach (ST) [2], the stub bundling approach (SB) [14] and the flow motion simulation approach (TNSS) [13]. The results are shown in Figure 11(c), Figure 12, and Table 1. From Figure 11(c), Figure 12, and Table 1, we can see that RFDA-FM has distinctive characteristics and specific advantages.

(1) RFDA-FM can generate flow maps with no acute flow-in angles, no overlaps between nodes and edges, and no edge crosses as ST and SB do. But TNSS and FD have 4 and 1 acute flow-in angles, and FD has 1 overlap between nodes and edges.

(2) RFDA-FM can produce visually smooth and natural edges as TNSS does. The mean value of visual smoothness indexes (*MSI*) for RFDA-FM₁, RFDA-FM₂, and RFDA-FM₃ is 0.751, 0.758, and 0.769 which are a little larger than TNSS and are larger than FD, ST, and SB. The reason is that slightly curved edges with small splitting angles will have large values on the visual smooth index (*S*), and curve difference necessity (*GC₂*) is considered in our approach. If curviness is the key to be considered, SB may be the best. But as Sun [13] pointed out, the SB layout had an artificial feeling with intentionally curved edges where they could be simply straight. Though the ST layout looks natural, it has the smallest *MSI* (0.621). The reason is that the splitting nodes in the ST layout are close to the destination nodes and the splitting angles are large [13].

(3) RFDA-FM is better at making nodes not close to the edges, and the distance between nodes and edges can be easily controlled with the parameter *t*. For example, if we set a larger *t*, RFDA-FM₃ (*t*=2) will have fewer nodes that are

within 100*10³m of their nearby edges than RFDA-FM₁ (*t*=1) and RFDA-FM₂ (*t*=1). By comparing to FD, ST, SB, and TNSS, RFDA-FM does have a larger distance between nodes and edges: RFDA-FM₂ has the largest *MDis_{min}* and RFDA-FM₃ has the least nodes which are within 100*10³m and 70*10³m of their nearby edges.

(4) ST has the smallest total length (*TL*) and RFDA-FM₂ has the second smallest *TL* because the two layouts both have more nodes that are close to their nearby edges. But compared to FD, ST, and SB, RFDA-FM₂ has the least nodes which are within 100*10³m and 70*10³m of their nearby edges. By comparing RFDA-FM₁ (a larger $\omega=0.65$) and RFDA-FM₃ (a larger *t*=2), the *TL* of RFDA-FM₁ and RFDA-FM₃ will increase, but they will have fewer nodes that are close to their nearby edges.

(5) SB has the largest mean value of the user preference index (*MUPI*). The reason may be that SB produces very smooth curves. The *MUPI* for RFDA-FM₁, RFDA-FM₂, and RFDA-FM₃ are 3.30, 3.04, and 3.43, which means that most of the users moderately prefer the generated layouts by RFDA-FM.

Based on the above analysis, we can see that no single approach is universally better than the others in terms of all the quality criteria in Section 3.2. For example, ST has the smallest total length (*TL*), and it also has many nodes which are close to their nearby edges; SB is the most preferred one by users, it also has an artificial feeling; TNSS has visually smooth and natural edges, it also has the largest *TL*. RFDA-FM can well meet all the quality criteria of the flow maps, namely smooth curves, no acute flow-in angles, no overlaps between nodes and edges, no edge crosses, and a moderately preferred tree-like layout with a clear hierarchy of branches as most listed approaches do. Specifically, RFDA-FM has the highest *MSI* and can be better at keeping destination nodes away from edges.

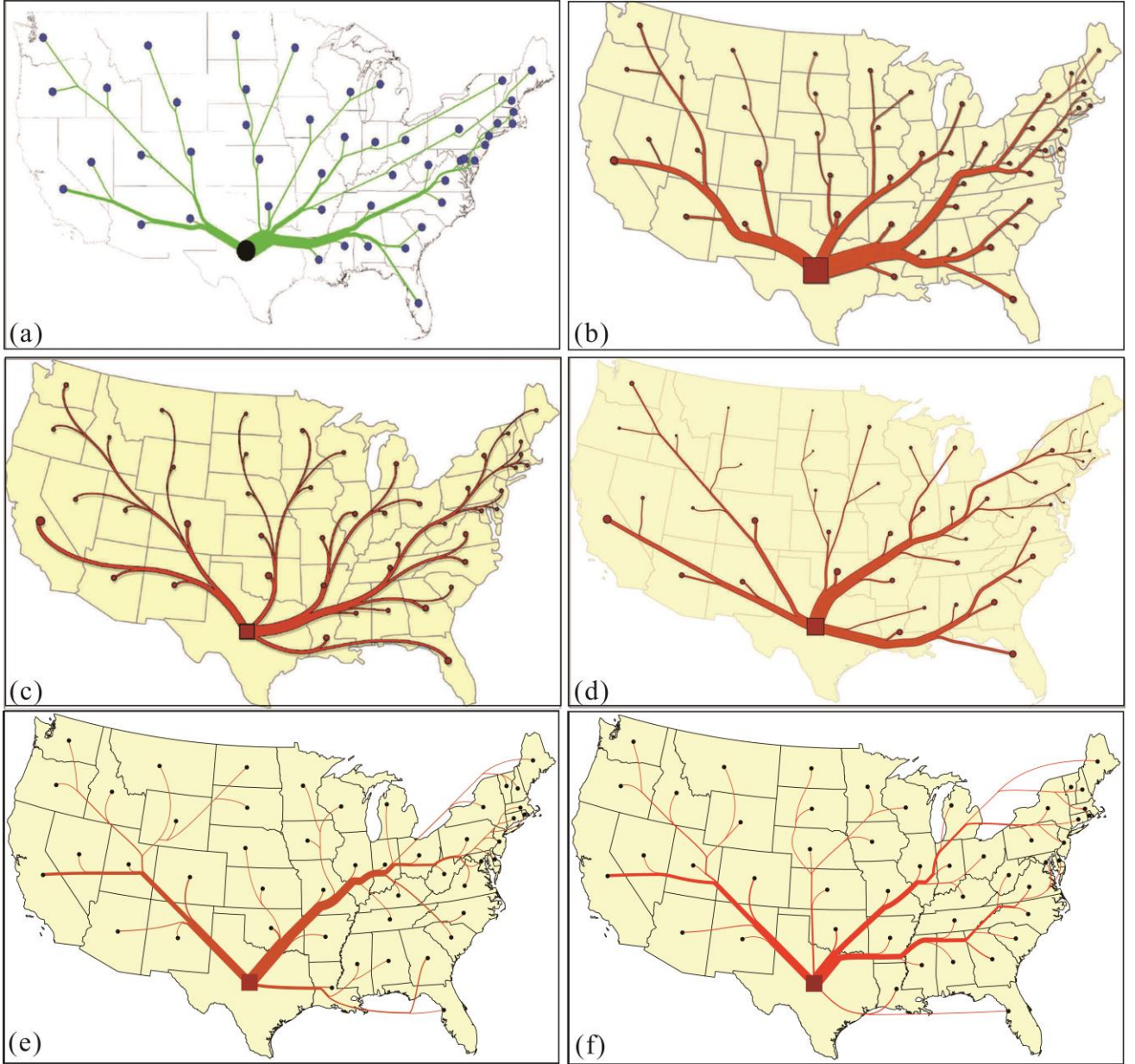


Figure 12. Flow maps for population migration from Texas to other states in the 2000 US Census by existing approaches. (a) The force-directed approach (FD) [15]; (b) The spiral tree approach (ST) [2]; (c) The stub bundling approach (SB) [14]; (d) The flow motion simulation approach (TNSS) [13]; (e) The new approach proposed in this article with $\omega=0.35$, $k=4$, $t=1$ (RFDA-FM₂); (f) The new approach proposed in this article with $\omega=0.65$, $k=4$, $t=2$ (RFDA-FM₃).

6 EXTENSIONS

In the above experiments, mapping spaces are all considered as being homogeneous, while mapping spaces with obstacle areas or heterogeneous mapping spaces are also widely used in practices [2, 13]. As illustrated in **Section 4.2**, our approach can also be applied to these two kinds of mapping spaces.

6.1 Case 1. Mapping space with obstacle areas

Population migration from California to other states in the 2000 US Census is taken as experiment data, in which the Great Salt Lake and part of the Mississippi river are taken as obstacle areas. Data source: <https://www.ipums.org/>; parameter settings are the same

as **Section 5.1**.

Results are shown in Figure 13 and Table 2. We observe that a result with no crosses between edges and obstacle areas can be successfully produced if the obstacle areas are considered. Similarly, the total length of the flow map will slightly increase by $0.07 \cdot 10^6 \text{m}$ (0.26%) due to cross avoidance. While if the obstacle areas are not considered, 2 crosses between edges and obstacle areas will be made, as shown in Area A of Figure 13(a). But the two generated flow maps with our approach can both well avoid node overlaps or edge crosses (except the crosses between edges and important objects), namely, meet the quality criteria in **Section 3.2**.

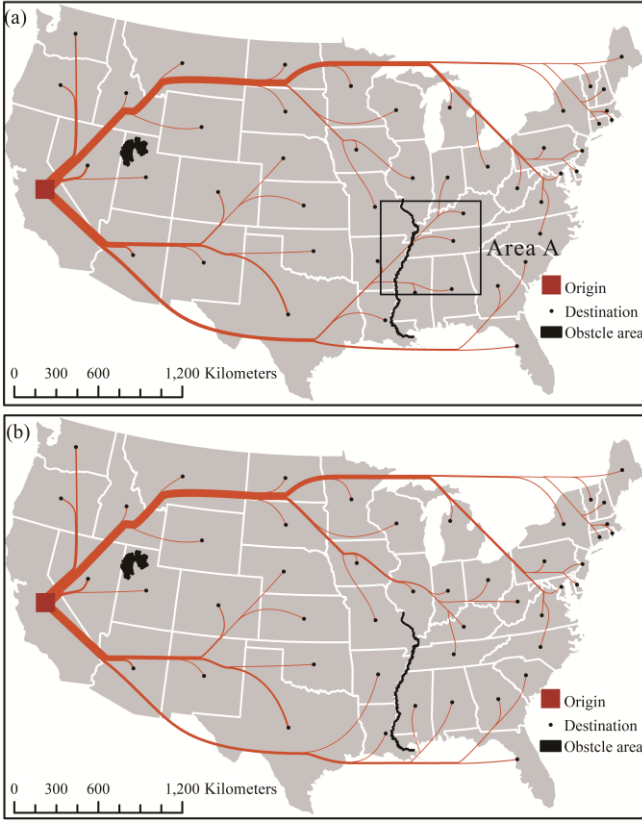


Figure 13. Flow map for population migration from California to other states in the 2000 US Census. (a) Without consideration of obstacle areas; (b) With consideration of obstacle areas.

6.2 Case 2. Heterogeneous mapping space

The good exports from Russia to other European countries ($\geq 0.1\%$) in 2019 are taken as experiment data, in which sea areas need to be avoided as much as possible to save transporting expenses, data source: <https://globalledge.msu.edu/countries/russia/tradestats/>; parameter settings are the same as Section 5.1. To avoid the sea areas as much as possible, the resolution of the grids in sea area (SR_s) is set as $SR_s = 1/3 * R_s$ (R_s is defined in Equation (1)). In the maze-solving algorithm, the mapping space is searched grid by grid. If a smaller R_s is set for sea areas, it means more steps are cost by searching across sea areas. The sea areas can then be avoided as much as possible.

From the results in Figure 14 and Table 2, we observe that a result with 5 fewer crosses (as shown in Areas A to E) between edges and sea areas can be successfully produced if the sea areas are considered. As for the 4 generated crosses between edges and sea areas in Figure 14 (b), these crosses are inevitably generated because these involved areas are apart from the main lands. Similarly, the total length of the flow map will slightly increase by $1.43 * 10^6 m$ (4.65%) due to sea area avoidance. But the two generated flow maps with our approach can both well avoid node overlaps or edge crosses, namely, meet the quality criteria in Section 3.2.

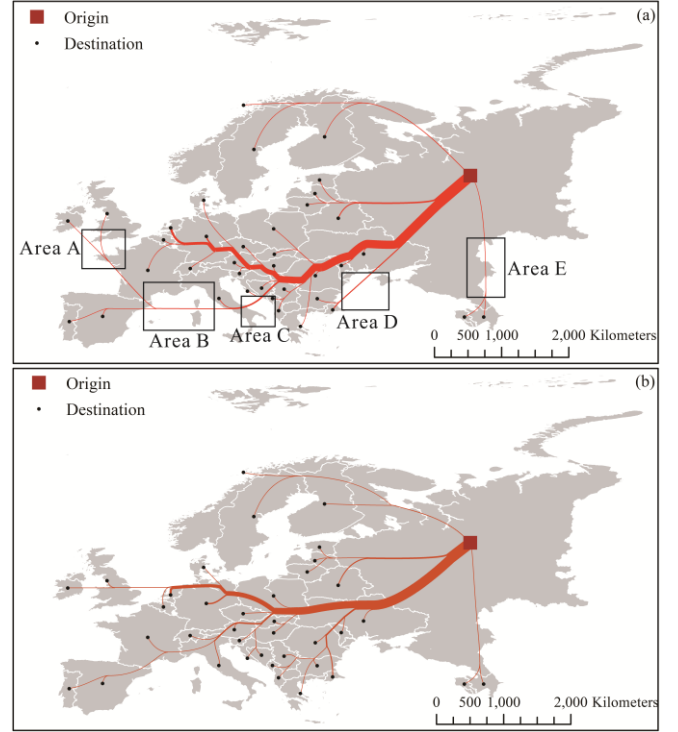


Fig. 14. Flow map for good exports from Russia to other European countries ($\geq 0.1\%$) in 2019. (a) Sea areas are not considered; (b) Sea areas need to be avoided as much as possible.

Table 2. Quantitative assessment on layout quality in different mapping spaces.

Measures	Obstacle areas		Mapping space	
	Without	With	Homo-gene-ous	Hetero-gene-ous
$TL (10^6 m) \downarrow$	27.30	27.37	30.74	32.17
$MSI \uparrow$	0.798	0.799	0.780	0.779
$MDIs (10^3 m)$				
$MDI_{min} \uparrow$	28.2	28.2	58.4	75.3
$n (MDIs < 100) \downarrow$	14	15	7	3
$n (MDIs < 70) \downarrow$	5	5	1	0
$n (MDIs < 40) \downarrow$	1	1	0	0
$n (MDIs < 20) \downarrow$	0	0	0	0
$FaN (< 120^\circ) \downarrow$	0	0	0	0
$ECN \downarrow$	0	0	0	0
$EON \downarrow$	0	0	0	0
$EIN \downarrow$	3	0	4	9

Note: If we consider the obstacle areas, EIN is the number of crosses between edges and obstacle areas; If we consider the heterogeneous mapping space (e.g., sea areas need to be avoided as much as possible), EIN is the number of crosses between edges and sea areas.

7 DISCUSSIONS

7.1 Strategy effectiveness analysis

To generate a satisfactory flow map layout, some strategies are applied in our approach and are summarized in Table 3. To validate the feasibility of these strategies, ablation experiments are performed. The baseline is the result for evaluation in Section 5.2, Figure 11(c). Three layouts without the strategies in Table 3 are then produced, as in

Figure 15. The statistical results are shown in Table 4.

Table 3. Strategies applied in our approach.

Name	Descriptions	Location
S_{t_1}	Path length refinement by considering the acute flow-in angle avoidance (RC_1).	Section 4.3.1.2
S_{t_2}	Searching range definition by considering overlaps avoidance and suitable distance maintenance between nodes and edges (RC_2 , RC_3).	Section 4.3.2.3
S_{t_3}	Path importance definition in which the flow path straightly connects to the origin is preferred, which helps minimize the total length.	Section 4.3.3

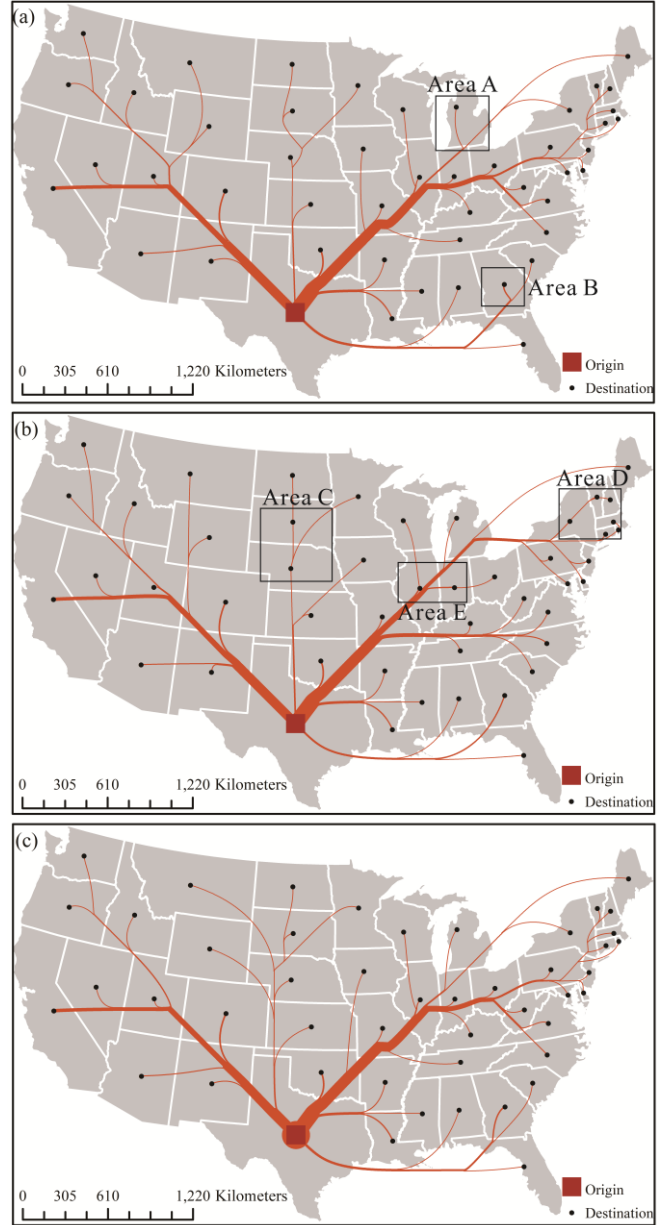
(1) S_{t_1} is applied to avoid acute flow-in angles. As shown in Figure 15(a) and Table 4, if S_{t_1} is not applied, 2 acute flow-in angles will be made. But if S_{t_1} is applied, the flow-in angles can be effectively avoided, as in Figure 11(c); But longer branches may be required to avoid acute flow-in angles, and the total length will slightly increase by 0.02×10^6 m (0.08%). Nevertheless, the layouts which are generated with or without S_{t_1} can all well meet the quality criteria in Section 3.2 (except the acute flow-in angles avoidance). Thus, we can conclude that S_{t_1} is effective to avoid acute flow-in angles, but it will also slightly increase the total length.

(2) S_{t_2} is applied to avoid overlaps and maintain suitable distances between nodes and edges. As shown in Figure 15(b) and table 4, if S_{t_2} is not applied, 7 overlaps between nodes and edges will be made, and 10 nodes with their distance to nearby edges less than 40×10^3 m. If S_{t_2} is applied, the overlaps between nodes and edges will be effectively avoided, Figure 11(c); and no nodes are with a distance to nearby edges less than 40×10^3 m; but longer edges may be required to avoid overlaps and maintain suitable distance between nodes and edges, the total length will increase 0.70×10^6 m (2.84%). These prove that S_{t_2} can effectively avoid overlaps and maintain suitable distance between nodes and edges, and the total length may also increase if S_{t_2} is applied.

(3) S_{t_3} is applied to minimize the total length of the flow map. By comparing Figure 11(c) and Figure 15(c), we can see that the total length will increase 1.19×10^6 m (4.83%) if S_{t_3} is not applied. Nevertheless, the layouts which are generated with or without S_{t_3} can both well meet the quality criteria in Section 3.2. These prove that S_{t_3} is very helpful to reduce the total length of a flow map.

Table 4. Quantitative assessment on layout quality for strategy effectiveness analysis.

Measures	S_{t_1}	S_{t_2}	S_{t_3}
TL (10^6 m) ↓	24.61	23.93	25.82
MSI ↑	0.757	0.772	0.767
$MDis$ (10^3 m)			
$MDis_{min}$ ↑	52.5	0	52.5
n ($MDis < 100$) ↓	15	16	13
n ($MDis < 70$) ↓	8	14	6
n ($MDis < 40$) ↓	0	10	0
n ($MDis < 20$) ↓	0	7	0
FaC ($< 120^\circ$) ↓	2	0	0
EEC ↓	0	0	0
EOC ↓	0	7	0

Figure 15. Flow maps for population migration from Texas to other states in the 2000 US Census which are produced without (a) S_{t_1} , (b) S_{t_2} , and (c) S_{t_3} .

7.2 Parameter sensitivity analysis

In this section, we analyze the influence of the parameter settings on the layouts and show how these parameters can intuitively control the layouts.

(1) ω in Equation (3)

ω is used to define the path length by considering the total length minimization (RC_3). Smaller ω means smaller total length (TL). We set $\omega=0.65$ in our experiment for evaluation and the result is shown in Figure 11(c). If a smaller ω is set ($\omega=0.35$), the paths from the destination nodes tend to flow in nearby paths, and the result is shown in Figure 12(e). If a larger ω is set ($\omega=1.0$), the paths from the destination nodes tend to flow in a location that is near the origin node, and the result is shown in Figure 16. The TL will increase with the increase of ω : the TL is 22.58×10^6 m if $\omega=0.35$, 24.63×10^6 m if $\omega=0.65$, and 41.95×10^6 m if $\omega=1.0$.

Similarly, the generated layouts will have longer branches with the increase of ω , as shown in Figures 11(c), 12(e), and 16. Furthermore, the nodes which are with small distance to their nearby edges will both increase with smaller or larger ω , and the $n(MDis < 100)$ is 17 if $\omega=0.35$, 25 if $\omega=1.0$, but 14 if $\omega=0.65$. Nevertheless, the generated layouts with different ω can all well meet the quality criteria in Section 3.2, e.g., no overlaps between nodes and edges and no edge crosses. If the users prefer a layout with a smaller total length, a smaller ω is recommended; if the users prefer a layout with longer branches, a larger ω is recommended.

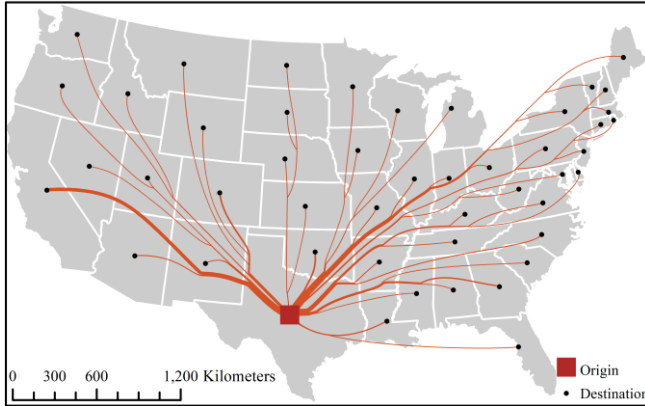


Figure 16. Flow maps for population migration from Texas to other states in the 2000 US Census with $\omega=1.0$.

(2) k in Equation (6)

k defines the k -order surrounding of the grid and is used for potential flow accumulation (Pf) computation. The direction to a grid with a higher Pf is prior to be searched in the maze-solving algorithm, which helps minimize the total length (TL). We set $k=1$ in our experiment for evaluation and the result is shown in Figure 11(c). The flow maps with $k=0$ (smaller k) or $k=8$ (larger k) are shown in Figure 17. As shown in Figures 11(c) and 17, we can see that the TL will both increase with smaller or larger k : the TL is $24.89 \times 10^6 m$ if $k=0$ and $24.74 \times 10^6 m$ if $k=8$, and the TL is $24.60 \times 10^6 m$ if $k=4$. Thus, a suitable k needs to be set in practice and $k=4$ is recommended. Nevertheless, the generated layouts with different ω can all well meet the quality criteria in Section 3.2.

(3) t for searching range definition considering overlap avoidance and suitable distance maintenance between nodes and edges (RC_3 and RC_5)

t is used to avoid overlaps and maintain suitable distance between nodes and edges (RC_3 and RC_5), and we set $t=1$ in our experiment for evaluation and the result is shown in Figure 11(c). If a smaller t is set ($t=0$), it means overlap avoidance is not considered, and the result is shown in Figure 15(b). Then 7 overlaps between nodes and edges will be made, and 10 nodes with their distance to nearby edges less than $40 \times 10^3 m$. If a larger t is set ($t=2$), the result is shown in Figure 12(f). Then the number of nodes that are within a small distance ($< 100 \times 10^3 m$) of their nearby edges will reduce, as 6 if $t=2$ and 15 if $t=1$. But if $t > 0$, no overlaps between nodes and edges will be made. The users can set a suitable t ($t > 0$) in practice according to their demands. If the users prefer a larger distance between

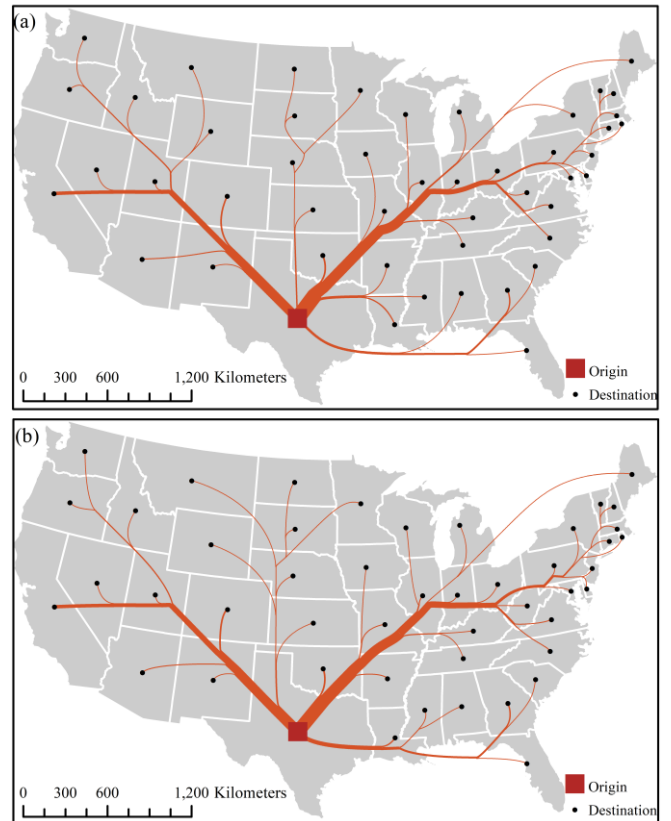


Figure 17. Flow maps for population migration from Texas to other states in 2000 US Census. (a) $k=0$; (b) $k=8$.

nodes and edges, a larger t is recommended.

(4) Other parameters

Some other parameters may also need to be set in the proposed approach e.g., the resolution (R_s) of the modeling DEM data, and the default priority of searching directions in the maze-solving algorithm. These parameters are set as default according to previous works. For example, large R_s will lead to an error because the closest points may fall into the same grid; while a small R_s may increase the computational cost. R_s is set as Equation (1) according to Hengl [43]. These parameters can also be set according to user demands.

7.3 Limitation analysis

Although suitable flow maps in different kinds of mapping spaces can be generated by using the proposed approach. It also has some limitations.

(1) The mapping space is modeled as a flat surface with the digital elevation model (DEM) and the grids in DEM data are assigned different types. But the elevation value is another key property in DEM data and is not considered in our approach. More complex flow data can be modeled with the DEMs if the elevation values are also considered. To improve the generalization ability of our approach, the elevation values need to be considered in our future works.

(2) As the flow paths are generated with an iterative process by a maze-solving algorithm. Thus, a result that meets the quality criteria as much as possible is just obtained each time, but not an optimal one. The result can be improved in our approach by introducing some other strategies, such as a backtracking strategy if unexpected results occur.

(3) Though the heterogeneous mapping space is considered in our approach, nodes of the mapping data may also distribute heterogeneously. For example, if the k -order surrounding definition for potential flow accumulation (Section 4.3.2.2) is adapted to different densities, different layouts may be produced.

(4) The proposed approach focuses on mapping data from one origin to many destinations. But in practice, data with multiple origins to many destinations or many origins to many destinations are also commonly used data, our approach needs to be extended for these data in future works.

(5) The generation of the flow map for the experiment data with 1 origin and 46 destinations will cost 6 minutes with the proposed approach. Though an approximate approach is also provided to reduce the search space in our uploaded code which can shorten the time to within 1 minute. More efficient strategies to speed up the proposed approach may need to be provided. Many efficient strategies have been introduced in digital elevation model data processing, and these strategies can also be applied to our approach.

8 CONCLUSIONS

In this paper, to generate a one-to-many flow map for visualization of movement data, we propose a river flow directions assignment algorithm over flat surfaces in digital elevation models (DEM) by modeling the mapping space as DEM data. Experiments indicate that the flow maps obtained by the proposed approach can achieve a higher quality in keeping nodes away from edges without node overlaps or edge crosses. Furthermore, the experiments demonstrate that our approach is also applicable to heterogeneous mapping space and mapping space with obstacle areas. Besides, the quality criteria can be intuitively controlled by setting parameters for users.

Future works will focus on: (1) Adaptive algorithm for different distributions of mapping data; (2) Visualization of flow map with multiple origins and dynamic data; (3) Improvement of algorithm efficiency.

ACKNOWLEDGMENTS

The authors wish to thank Tingzhong Huang for his help in data collection and Yalong Yang for sharing his JavaScript code. This work was supported in part by a grant from The National Natural Science Foundation of China (No.41871378) and The Research Development Fund of Zhejiang A & F University (2020FR083).

REFERENCES

- [1] A. H. Robinson. The 1837 maps of Henry Drury Harness. *The Geographical Journal*, 121(4): pp.440–450, 1955.
- [2] K. Buchin, B. Speckmann, and K. Verbeek. Flow map layout via spiral trees. *IEEE transactions on visualization and computer graphics*, 17(12), 2536-2544, 2011.
- [3] M. Castells and C. Blackwell. The information age: economy, society and culture. Volume 1. The rise of the network society. *Environment and Planning B: Planning and Design*, 25, 631-636, 1998.
- [4] S. Schöttler, Y. Yang, H. Pfister and B. Bach. Visualizing and interacting with geospatial networks: A survey and design space// *Computer Graphics Forum*. 2021.
- [5] D. Guo and X. Zhu. Origin-destination flow data smoothing and mapping. *IEEE Transactions on Visualization and Computer Graphics*, 20(12): 2043-2052, 2014.
- [6] Y. Yang, T. Dwyer, B. Jenny, et al. Origin-destination flow maps in immersive environments. *IEEE transactions on visualization and computer graphics*, 25(1): 693-703, 2018.
- [7] D. Phan, L. Xiao, R. Yeh, et al. Flow map layout. *IEEE Symposium on Information Visualization (INFOVIS 2005)*. IEEE, 219-224, 2005.
- [8] H. Zhou, P. Xu, X. Yuan, et al. Edge bundling in information visualization. *Tsinghua Science and Technology*, 18(2): 145-156, 2013.
- [9] B. Jenny, D. M. Stephen, I. Muehlenhaus, et al. Force directed layout of origin-destination flow maps. *International Journal of Geographical Information Science*, 31(8), 1521–1540, 2017.
- [10] J. Wood, J. Dykes and A. Slingsby. Visualization of origins, destinations and flows with OD maps. *The Cartographic Journal*, 47(2), 117–129, 2010.
- [11] X. Zhu and D. Guo. Mapping large spatial flow data with hierarchical clustering. *Transactions in GIS*, 18(3), 421–435, 2014.
- [12] Y. Yang, T. Dwyer, S. Goodwin, et al. Many-to-many geographically-embedded flow visualisation: An evaluation. *IEEE transactions on visualization and computer graphics*, 23(1): 411-420, 2016.
- [13] S. Sun. A spatial one-to-many flow layout algorithm using triangulation, approximate Steiner trees, and path smoothing. *Cartography and Geographic Information Science*, 46(3): 243-259, 2019.
- [14] A. Nocaj and U. Brandes. Stub bundling and confluent spirals for geographic networks. *International Symposium on Graph Drawing*. Springer, Cham: 388-399, 2013.
- [15] A. Debiasi, B. Simões and R. De Amicis. Force directed flow map layout. *2014 International Conference on Information Visualization Theory and Applications (IVAPP)*. IEEE, 170-177, 2014.
- [16] A. Debiasi, B. Simões and R. De Amicis. Supervised force directed algorithm for the generation of flow maps. WSCG 2014 22nd International Conference on Computer Graphics, Visualization and Computer Vision 2014b Plzen, Czech Republic.
- [17] S. Sun. An automated spatial flow layout algorithm using triangulation, approximate Steiner tree, and path smoothing[C]. *AutoCarto*, 2016.
- [18] S. K. Jensen and J. O. Domingue. Extracting topographic structure from digital elevation data for geographic information system analysis. *Photogrammetric engineering and remote sensing*. 54, 1593–1600, 1988.
- [19] J. Garbrecht and L. W. Martz. The assignment of drainage direction over flat surfaces in raster digital elevation models. *Journal of hydrology*. 193, 204–213, 1997.
- [20] P. Soille, J. Vogt and R. Colombo. Carving and adaptive drainage enforcement of grid digital elevation models. *Water resources research*. 39, 1366, 2003.
- [21] H. Zhang and G. Huang. Building channel networks for flat regions in digital elevation models. *Hydrological Processes: An International Journal*. 23, 2879–2887, 2009.
- [22] R. Barnes, C. Lehman and D. Mulla. An efficient assignment of drainage direction over flat surfaces in raster digital elevation models. *Computers & Geosciences*. 62, 128–135, 2014.
- [23] X. Liu, N. Wang, J. Shao, et al. An automated processing algorithm for flat areas resulting from DEM filling and interpolation. *ISPRS International Journal of Geo-Information*, 6(11): 376, 2017.

- [24] A. Tribe. Automated recognition of valley lines and drainage networks from grid digital elevation models: a review and a new method. *Journal of hydrology*, 139, 263–293, 1992.
- [25] H. Zhang, Z. Yao, Q. Yang, et al. An integrated algorithm to evaluate flow direction and flow accumulation in flat regions of hydrologically corrected DEMs. *Catena*, 151: 174–181, 2017.
- [26] Q. Zhu, Y. Tian and J. Zhao. An efficient depression processing algorithm for hydrologic analysis. *Computers & Geosciences*, 32, 615–623, 2006.
- [27] L. Wang and H. Liu. An efficient method for identifying and filling surface depressions in digital elevation models for hydrologic analysis and modelling. *International Journal of Geographical Information Science*, 20, 193–213, 2006.
- [28] R. Barnes, C. Lehman and D. Mulla. Priority-flood: an optimal depression-filling and watershed-labeling algorithm for digital elevation models. *Computers & Geosciences*, 62, 117–127, 2014.
- [29] C. Su, X. Wang, C. Feng, et al. An integrated algorithm for depression filling and assignment of drainage directions over flat surfaces in digital elevation models. *Earth Science Informatics*, 1–11, 2015.
- [30] C. Su, C. Feng, X. Wang, et al. An efficient algorithm for assignment of flow direction over flat surfaces in raster DEMs based on distance transform. *Earth Science Informatics*, 1–9, 2016.
- [31] W. Yu, C. Su, C. Yu, et al. An efficient algorithm for depression filling and flat-surface processing in raster DEMs. *IEEE Geoscience and Remote Sensing Letters*, 12, 424–428, 2014.
- [32] I. Florinsky. Digital terrain analysis in soil science and geology. Academic Press, 2016.
- [33] L. Wang, T. Ai, Y. Shen, et al. The isotropic organization of DEM structure and extraction of valley lines using hexagonal grid. *Transactions in GIS*, 24(2): 483–507, 2020.
- [34] A. H. Robinson. Early thematic mapping in the history of cartography. University of Chicago Press, Chicago, 1982.
- [35] W. R. Tobler. Experiments In Migration Mapping By Computer. *Cartography and Geographic Information Science*, 14(2):155–163, 1987.
- [36] S. van den Elzen and J. J. van Wijk. Multivariate network exploration and presentation: From detail to overview via selections and aggregations. *IEEE Transactions on Visualization and Computer Graphics*, 20(12):2310–2319, 2014.
- [37] K. Buchin, B. Speckmann and K. Verbeek. Angle restricted Steiner arborescences for flow map layout. *Algorithmica*, 72(2), 656–685, 2015.
- [38] B. Jenny, D. M. Stephen, I. Muehlenhaus, et al. Design principles for origin-destination flow maps. *Cartography and Geographic Information Science*, 45(1): 62–75, 2018.
- [39] W. Dong, S. Wang, Y. Chen, et al. Using eye tracking to evaluate the usability of flow maps. *ISPRS International Journal of Geo-Information*, 7(7): 281, 2018.
- [40] K. Xu, C. Rooney, P. Passmore, et al. A user study on curved edges in graph visualization[J]. *IEEE transactions on visualization and computer graphics*, 2012, 18(12): 2449–2456.
- [41] D. Holten and J. J. van Wijk. A user study on visualizing directed edges in graphs. *Paper presented at the CHI '09 SIGCHI Conference on Human Factors in Computing Systems*, Boston, 2009.
- [42] C. Bennett, J. Ryall, L. Spalteholz, et al. The aesthetics of graph visualization. In D. W. Cunningham, G. Meyer, & L. Neumann (Eds), *Computational Aesthetics'07: Proceedings of the Third Eurographics conference on Computational Aesthetics in Graphics, Visualization and Imaging* (pp. 57–74). Aire, 2007.
- [43] C. Ware, H. Purchase, L. Colpoys, et al. Cognitive measurements of graph aesthetics. *Information Visualization*, 1(2), 103–110, 2002.
- [44] W. Huang, S. H. Hong and P. Eades. Effects of crossing angles. *Paper presented at the Visualization Symposium, PacificVIS '08*. IEEE Pacific, Kyoto, 2008.
- [45] W. Huang, P. Eades and S. H. Hong. Larger crossing angles make graphs easier to read. *Journal of Visual Languages & Computing*, 25(4), 452–465, 2014.
- [46] X. Zhang, J. Stoter, T. Ai, et al. Automated evaluation of building alignments in generalized maps[J]. *International journal of geographical information science*, 2013, 27(8): 1550–1571.
- [47] T. Hengl. Finding the right pixel size. *Computers & geosciences*, 32(9): 1283–1298, 2006.
- [48] D. M. Willardson. Analysis of micro mouse maze solving algorithm. *Learning From Data*, 2001.
- [49] J. F. O'Callaghan and D. M. Mark. The extraction of drainage networks from digital elevation data. *Computer Vision, Graphics, & Image Processing*, 28(3), 323–344, 1984.
- [50] R. Chernobelskiy, K. I. Cunningham, M. T. Goodrich, et al. Force-directed Lombardi-style graph drawing[C]//International Symposium on Graph Drawing. Springer, Berlin, Heidelberg, 2011: 320–331.
- [51] Z. Wei, Y. Liu, L. Cheng, et al. A Progressive and Combined Building Simplification Approach with Local Structure Classification and Backtracking Strategy. *ISPRS International Journal of Geo-Information*, 10(5): 302, 2021.
- [52] S. Ruggles, S. Flood, S. Foster, et al. IPUMS USA: Version 11.0 [dataset]. Minneapolis, MN: IPUMS, 2021. <https://doi.org/10.18128/D010.V11.0>
- [53] Z. Wei, Q. Guo, L. Wang, et al. On the spatial distribution of buildings for map generalization. *Cartography and Geographic Information Science*, 45(6): 539–555, 2018.

ZHIWEI WEI received a Ph.D. degree in cartography and geographic information science from Wuhan University in 2020. He is currently an assistant professor at the Aerospace Information Research Institute, Chinese Academy of Sciences, Beijing, China. His research interests include automatic map generalization, automatic map design, and spatial data visualization.

SU DING received a Ph.D. degree in geography from Wuhan University in 2020. She is currently an assistant professor at the College of Environmental and Resource Sciences, Zhejiang A & F University. Her research interests include geospatial information analysis and modeling, and spatial data mining.

WENJIA XU received a Ph.D. degree in signal and information processing from the University of Chinese Academy of Sciences in 2021. She also worked as a visiting Ph.D. student at the Max-Planck Institute for Informatics in Saarbrücken, Germany between 2019–2020. She is currently a research associate professor at the School of Information and Communication Engineering, Beijing University of Posts and Telecommunications. Her research interest includes learning with limited supervision for computer vision tasks, explainable machine learning, and data visualization.

YUANBEN ZHANG received a B.S. degree from the University of Science and Technology of China in 2011, and an M.S. degree from the Institute of Electronics, Chinese Academy of Science, Beijing, China in 2014. He is currently an assistant professor at the Aerospace Information Research Institute, Chinese Academy of Sciences, Beijing, China. His research interests include geospatial data mining and visualization analysis.

YANG WANG received a Ph.D. degree in graphics from Peking university in 2014. She is currently an associate professor and a master advisor at the Aerospace Information Research Institute, Chinese Academy of Sciences, Beijing, China. Her research interests include geospatial information analysis and visualization.